

Electron-phonon effects on spin-orbit split bands of two-dimensional systems

E. Cappelluti,^{1,2} C. Grimaldi,^{3,4} and F. Marsiglio⁵

¹*SMC Research Center, INFN-CNR c/o Department of Physics, University "La Sapienza," P.le A. Moro 2, 00185 Roma, Italy*

²*Istituto dei Sistemi Complessi (ISC), CNR, v. dei Taurini 19, 00185 Roma, Italy*

³*Max-Planck-Institut für Physik Komplexer Systeme, Nöthnitzer Strasse 38, D-01187 Dresden Germany*

⁴*LPM, Ecole Polytechnique Fédérale de Lausanne, Station 17, CH-1015 Lausanne, Switzerland*

⁵*Department of Physics, University of Alberta, Edmonton, Alberta, Canada T6G 2J1*

(Received 22 March 2007; revised manuscript received 17 July 2007; published 21 August 2007)

The electronic self-energy is studied for a two-dimensional electron gas coupled to a spin-orbit Rashba field and interacting with dispersionless phonons. For the case of a momentum independent electron-phonon coupling (Holstein model) we solve numerically the self-consistent noncrossing approximation for the self-energy and calculate the electron mass enhancement m^*/m and the spectral properties. We find that, even for nominal weak electron-phonon interaction, for strong spin-orbit couplings the electrons behave as effectively strongly coupled to the phonons. We interpret this result by a topological change of the Fermi surface occurring at sufficiently strong spin-orbit coupling, which induces a square-root divergence in the electronic density of states at low energies. We provide results for m^*/m and for the density of states of the interacting electrons for several values of the electron filling and of the spin-orbit interaction.

DOI: [10.1103/PhysRevB.76.085334](https://doi.org/10.1103/PhysRevB.76.085334)

PACS number(s): 73.20.At, 71.38.-k, 71.70.Ej

I. INTRODUCTION

Prompted by considerable technological interests, the physics of itinerant electrons coupled to spin-orbit (SO) potentials has been the subject of extensive investigations in recent years.^{1,2} In materials of interest, the main sources of SO coupling are the Rashba interaction arising from structural inversion asymmetries of low-dimensional structures,³ and the Dresselhaus interaction present in bulk crystals lacking inversion symmetry.⁴ Depending on the material characteristics, one of the above interactions, or even both, may be present, lifting the spin degeneracy of the electron dispersion. When measured at the Fermi level, the resulting energy splitting Δ_{SO} is commonly used to estimate the strength of the SO interaction.

In narrow-gap III-V semiconductor-based heterostructures, such as GaAs and InAs quantum wells, Δ_{SO} is a few meV, while in II-VI quantum wells Δ_{SO} is greatly enhanced. For example, the heavy-hole conduction band of HgTe displays SO splitting values ranging between 10–17 meV and 30 meV.^{5,6} Much stronger SO splittings have been observed in the surface states of metals⁷ and semimetals,^{8,9} and the corresponding Δ_{SO} may be so large, e.g., $\Delta_{\text{SO}} \approx 110$ meV in Au(111),⁷ that the possibility of detecting SO split image states has been recently put forward.¹⁰ Other systems displaying giant SO splittings are surface alloys as, for example, Li/W(110),¹¹ Pb/Ag(111),^{12,13} and Bi/Ag(111),¹⁴ or even one-dimensional structures such as Au chains in vicinal Si(111) surfaces.¹⁵ For such low-dimensional or structured materials, the SO interaction is of Rashba type, but large SO splittings have been found (or predicted) also in bulk crystals, where the Dresselhaus interaction leads to Δ_{SO} as large as 200 meV in noncentrosymmetric superconductors CePt₃Si,^{16,17} Li₂Pd₃B, and Li₂P₇B.^{18,19}

Such strong SO couplings may possibly have interesting applications in spintronic devices, but represent also a compelling and challenging problem from the theoretical stand-

point, in particular when Δ_{SO} is no longer the smallest energy scale in the system, as in III-V semiconductor heterostructures where $\Delta_{\text{SO}} \approx 1\text{--}5$ meV, but competes in magnitude with other characteristic energy scales such as the phonon frequency or the Fermi energy. From this perspective, systems such as the Bi/Ag(111) surface alloy, which shows bands split by about 200 meV,^{13,14} are particularly promising, given also the alleged possibility of tuning, by Pb doping, the Fermi energy E_F to values lower than the SO energy splitting.²⁰

A few novel and interesting features arising from strong SO splittings have already been investigated theoretically in the literature. For example, in Ref. 21 it has been demonstrated that the Rashba SO coupling induces an infinite number of bound states in two dimensions, even for short ranged impurity potentials, while in a recent work we have shown that the superconducting critical temperature of a low-density two-dimensional (2D) electron gas can be significantly enhanced by the Rashba interaction.²² Both phenomena discussed in Refs. 21 and 22 can be understood in terms of a SO induced topological change of the Fermi surface, which gives rise to an effective reduction of dimensionality of the electronic density of states for E_F sufficiently smaller than the SO characteristic energy.

In this paper we analyze the effects of such topological change of the Fermi surface on the electron-phonon (el-ph) problem of 2D systems. In particular, we study one-particle spectral properties and extract the combined el-ph and SO effects on the electronic effective mass m^* and on the interacting density of states (DOS). We show that, even for weak or moderate couplings to phonons, the effective reduction of the bare DOS induced by the Rashba interaction leads to a strong increase of m^* , and to phonon satellite peaks in the interacting DOS, which are typical signatures of an effectively strong el-ph coupling. Due to the two-dimensionality of our model, and to the Rashba type of SO coupling, our results could be relevant for both metal and semimetal sur-

face states, for which the el-ph interaction has been shown to be relevant,^{9,23–26} and for surface superconductors,²⁷ with the hypothesis that pairing is provided by the coupling to phonons.

II. RASHBA-HOLSTEIN MODEL

Two-dimensional quantum wells, with strong and asymmetric confining potentials, and surface states with weak or negligible coupling to the bulk can be satisfactorily represented by the following 2D electron Hamiltonian with SO interaction:

$$H_0 = \sum_{\mathbf{k}\alpha} \epsilon_{\mathbf{k}} c_{\mathbf{k}\alpha}^\dagger c_{\mathbf{k}\alpha} + \sum_{\mathbf{k}\alpha\beta} \Omega_{\mathbf{k}} \cdot \sigma_{\alpha\beta} c_{\mathbf{k}\alpha}^\dagger c_{\mathbf{k}\beta}, \quad (1)$$

where $c_{\mathbf{k}s}^\dagger$ ($c_{\mathbf{k}s}$) is the creation (annihilation) operator for an electron with momentum $\mathbf{k}=(k_x, k_y)$ and spin index $\alpha = \uparrow, \downarrow$. In the above expression, $\epsilon_{\mathbf{k}}$ is the electron dispersion in the absence of SO coupling, σ is the spin-vector operator with components $(\sigma^x, \sigma^y, \sigma^z)$ given by the Pauli matrices, and $\Omega_{\mathbf{k}}$ is a \mathbf{k} dependent SO pseudopotential arising from the asymmetry in the z direction of the confining potential. Here we consider a linear Rashba model for the SO interaction

$$\Omega_{\mathbf{k}} \cdot \sigma = \gamma(k_x \sigma^y - k_y \sigma^x), \quad (2)$$

where γ is the SO coupling constant. Furthermore, we assume that the unperturbed electron band is parabolic, $\epsilon_{\mathbf{k}} = \hbar^2 k^2 / 2m$, where m is the band mass of the electron. Apart from a constant shift E_0 (defined below) which can be absorbed in the chemical potential, the eigenvalues of Eqs. (1) and (2) are

$$E_k^s = \frac{\hbar^2}{2m} (k + s k_0)^2, \quad (3)$$

where $k = |\mathbf{k}|$, $s = \pm$ is the chirality number, and k_0 is the Rashba momentum

$$k_0 = \frac{m}{\hbar^2} \gamma. \quad (4)$$

The two electron branches E_k^\pm are plotted in Fig. 1(a) in units of the Rashba energy

$$E_0 = \frac{\hbar^2 k_0^2}{2m} = \frac{m}{2\hbar^2} \gamma^2 \quad (5)$$

which corresponds to the energy difference between the degeneracy point at $k=0$ and the bottom of the lower band at $k=k_0$. In Fig. 1(a) we indicate also the Fermi levels for the $E_F > E_0$ and $E_F < E_0$ cases (horizontal dashed lines) which represent two qualitatively different situations. For $E_F > E_0$, the Fermi level crosses bands of different chirality and the corresponding Fermi sea is given by the area of two concentric Fermi circles, as sketched in Fig. 1(a). In this case, the corresponding DOS for each subband is

$$N_\pm(E_F) = N_0 \left(1 \mp \sqrt{\frac{E_0}{E_F}} \right) \quad \text{for } E_F \geq E_0, \quad (6)$$

where $N_0 = m / 2\pi\hbar^2$ is the DOS per spin direction with zero SO coupling. The sum over the two chiral states $N(E_F)$

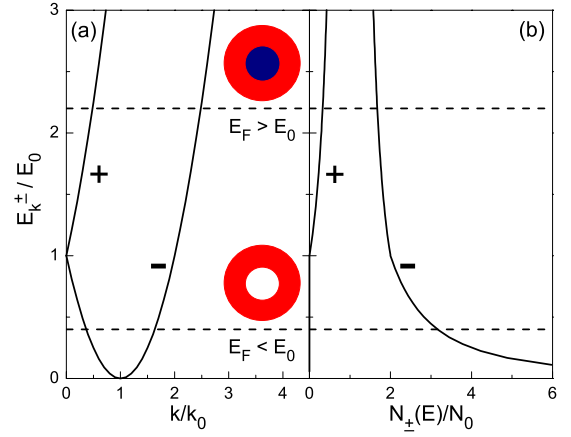


FIG. 1. (Color online) (a) Electron dispersion $E_k^\pm = \frac{\hbar^2}{2m} (k \pm k_0)^2$ for a spin-orbit split electron gas. The energy $E_0 = \frac{m}{2\hbar^2} \gamma^2$ is a measure of the spin-orbit interaction and is equivalent to the minimum interband excitation energy for an electron sitting at the bottom of the lower band. The upper and lower horizontal dashed lines indicate the position of the Fermi level for $E_F > E_0$ and $E_F < E_0$, respectively. Also shown are the corresponding Fermi circles with occupied states drawn by gray (colored) regions. (b) Density of states plotted from Eqs. (6) and (7).

$= N_+(E_F) + N_-(E_F)$ is therefore identical to the total DOS $2N_0$ of a 2D electron gas without SO interaction [Fig. 1(b)]. Furthermore, in the $E_F \gg E_0$ regime, one has $N_\pm(E_F) \approx N_0$, and the dispersions of the low excitations in the vicinity of E_F can be approximated by $v_F(k - k_F) \pm \Delta_{\text{SO}}/2$, where v_F and k_F are, respectively, the Fermi velocity and momentum in the absence of SO interaction and $\Delta_{\text{SO}} = 2\gamma k_F$ is the SO energy splitting. This is the quantity which is usually used to quantify the SO strength in semiconductors such as GaAs and InAs.

For $E_F < E_0$ the situation is drastically different. In this case in fact, as shown in Fig. 1(a), the Fermi level crosses only the $s = -1$ band but, since E_k^- has a minimum at $k = k_0 \neq 0$, the Fermi surface is still constituted by two concentric circles. The resulting Fermi sea is therefore given by the area of the annulus comprised by the two circles and in the limit of $E_F \rightarrow 0$, with $E_0 \neq 0$, the Fermi surface S_F coalesces into a circle of radius k_0 , $S_F = 2\pi k_0$, while the Fermi velocity v_F vanishes as $\sqrt{E_F}$. Since $N(E_F) \propto S_F / v_F$, the resulting DOS is therefore²²

$$N(E_F) = N_-(E_F) = 2N_0 \sqrt{\frac{E_0}{E_F}} \quad \text{for } E_F < E_0. \quad (7)$$

As we shall see in the following, the one-dimensional-like singularity of Eq. (7) has important and peculiar effects on the low-energy properties of the system, in contrast with the $E_F > E_0$ case, for which the corresponding DOS is featureless.

Let us introduce now the coupling to the phononic degrees of freedom. In the present paper, we consider the following Holstein-type of interaction Hamiltonian:

$$H_{\text{ph}} = \sum_{\mathbf{q}} \omega_{\mathbf{q}} a_{\mathbf{q}}^{\dagger} a_{\mathbf{q}} + g \sum_{\mathbf{k}\mathbf{k}'\alpha} c_{\mathbf{k}\alpha}^{\dagger} c_{\mathbf{k}'\alpha} (a_{\mathbf{k}-\mathbf{k}'}^{\dagger} + a_{\mathbf{k}'-\mathbf{k}}), \quad (8)$$

where $a_{\mathbf{q}}^{\dagger}$ ($a_{\mathbf{q}}$) is the creation (annihilation) operator for a phonon with momentum \mathbf{q} , $\omega_{\mathbf{q}}$ is a dispersionless phonon frequency, and g is the momentum independent el-ph matrix element. As will become clear in the following, the choice of the momentum independent quantities $\omega_{\mathbf{q}}$ and g is convenient for the calculation of the self-energy, and permits a more direct evaluation of the effects of the SO interaction on the el-ph properties. The present analysis is therefore a starting point for more general formulations of the el-ph Hamiltonian.

The thermal Green's function of the electrons subjected to the total Hamiltonian $H=H_0+H_{\text{ph}}$ satisfies the following Dyson equation:

$$\mathbf{G}(\mathbf{k}, i\omega_n) = [\mathbf{G}_0^{-1}(\mathbf{k}, i\omega_n) - \Sigma(\mathbf{k}, i\omega_n)]^{-1}, \quad (9)$$

where $\omega_n = (2n+1)\pi T$ is a fermionic Matsubara frequency and T is the temperature. $\mathbf{G}_0(\mathbf{k}, i\omega_n)$ is the noninteracting electron propagator and $\Sigma(\mathbf{k}, i\omega_n)$ is the self-energy due to the coupling with phonons. Due to the SO interaction appearing in H_0 , these quantities are 2×2 matrices in the spin subspace. From Eqs. (1) and (2), the noninteracting propagator is

$$\mathbf{G}_0(\mathbf{k}, i\omega_n) = \frac{1}{2} \sum_{s=\pm 1} (1 + s\hat{\Omega}_{\mathbf{k}} \cdot \sigma) G_0(E_k^s, i\omega_n), \quad (10)$$

where $\hat{\Omega}_{\mathbf{k}} \cdot \sigma = \hat{k}_x \sigma_y - \hat{k}_y \sigma_x$, and $G_0(E_k^s, i\omega_n) = 1/(i\omega_n - E_k^s + \mu)$, where μ is the chemical potential.

For the evaluation of the self-energy, we shall consider a self-consistent Born approximation (noncrossing approximation) which neglects all el-ph vertex corrections. Furthermore, we shall not consider many-body corrections to the phonon propagator. These limitations will be discussed in Sec. V and, for the moment, it suffices to keep in mind that this approximation scheme should be not too poor as long as the coupling to the phonons is sufficiently weak. Hence, given the phonon propagator

$$D(i\omega_n - i\omega_m) = \frac{\omega_0^2}{(i\omega_n - i\omega_m)^2 - \omega_0^2}, \quad (11)$$

the resulting electron self-energy matrix in the noncrossing approximation reduces to

$$\Sigma(\mathbf{k}, i\omega_n) = -\frac{\lambda}{N_0} T \sum_m \int \frac{d\mathbf{k}'}{(2\pi)^2} D(i\omega_n - i\omega_m) \mathbf{G}(\mathbf{k}', i\omega_m), \quad (12)$$

where $\lambda = 2g^2 N_0 / \omega_0$ is the el-ph coupling constant. From Eq. (12) it is clear that, due to the momentum independence of the el-ph interaction, the self-energy (12) depends only upon the frequency. Furthermore, by substituting $\mathbf{G}_0(\mathbf{k}', i\omega_m)$ for $\mathbf{G}(\mathbf{k}', i\omega_m)$ in Eq. (12), the resulting second-order self-energy is diagonal in the spin space. This holds true for all orders of iteration, so that $\Sigma(\mathbf{k}, i\omega_n) = \Sigma(i\omega_n) \mathbf{1}$, where $\mathbf{1}$ is the unit matrix. The Green's function (9) can therefore be rewritten as

$$\mathbf{G}(\mathbf{k}, i\omega_n) = \frac{1}{2} \sum_{s=\pm 1} (1 + s\hat{\Omega}_{\mathbf{k}} \cdot \sigma) G(E_k^s, i\omega_n), \quad (13)$$

where

$$G(E_k^s, i\omega_n) = \frac{1}{i\omega_n - E_k^s + \mu - \Sigma(i\omega_n)}, \quad (14)$$

is the electron propagator in the chiral basis for the interacting case while the self-energy is

$$\Sigma(i\omega_n) = -\lambda T \sum_m D(i\omega_n - i\omega_m) g(i\omega_m), \quad (15)$$

where

$$g(i\omega_m) = \frac{1}{2N_0} \sum_s \int_0^{k_c} \frac{dkk}{2\pi} G(E_k^s, i\omega_m). \quad (16)$$

In the above expression, we have introduced an upper momentum cutoff k_c which prevents the integral over k from diverging. Such divergence is an artifact due to the use of a momentum independent el-ph matrix element g in Eq. (8) and of the electron gas model of H_0 . On physical grounds, the introduction of k_c is equivalent therefore to defining a finite Brillouin zone of area πk_c^2 or, equivalently, a finite bandwidth $E_c = \hbar^2 k_c^2 / 2m$ when $E_0 = 0$. In the following, E_c will be chosen to be much larger than the other relevant energy scales of the system ($E_c \gg \omega_0, E_0, E_F$). A finite k_c , or E_c , also permits us to define a finite electron density $\rho_e = \sum_{\sigma} \int d\mathbf{k} / (2\pi)^2 \langle c_{\mathbf{k}\sigma}^{\dagger} c_{\mathbf{k}\sigma} \rangle$ which, relative to the cutoff k_c , becomes

$$\rho_e = \sum_s \int_0^{k_c} \frac{dkk}{2\pi} T \sum_n G(E_k^s, i\omega_n) e^{i\omega_n 0^+} = \frac{k_c^2}{4\pi} + T \sum_n \text{Re } g(i\omega_n), \quad (17)$$

where 0^+ is an infinitesimal positive quantity and the second equality has been obtained by using $T \sum_n G(E_k^s, i\omega_n) e^{i\omega_n 0^+} = 1/2 + T \sum_n \text{Re } G(E_k^s, i\omega_n)$.²⁸ In the following, we shall present results in terms of the electron number density

$$n_e = \frac{4\pi\rho_e}{k_c^2} \quad (18)$$

which attains the limiting value $n_e = 2$ ($n_e = 0$) for completely filled (empty) bands.

Before turning to the next sections, where we present our numerical results, it is worthwhile showing how the SO effects on the DOS enter the self-energy function. By transforming the integration over k in an integration over the energy, Eq. (16) can be rewritten as follows:

$$g(i\omega_m) = \int_0^{E_c} dE \rho_0(E) G(E, i\omega_m), \quad (19)$$

where, for simplicity, terms of order $\sqrt{E_0/E_c}$ have been omitted in the upper limit of integration, and

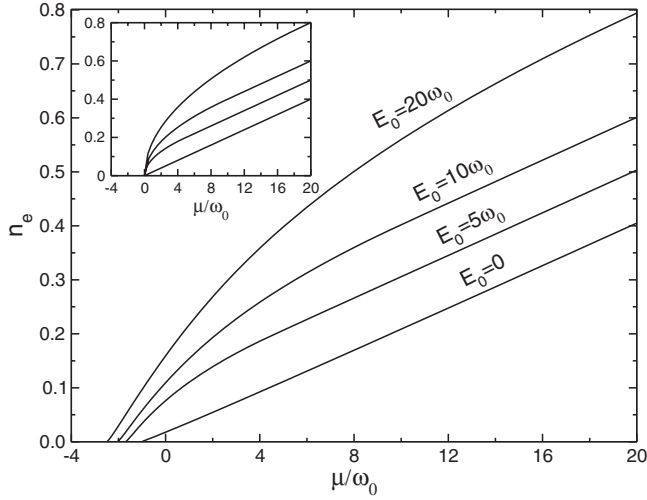


FIG. 2. Electron density number n_e as a function of the bare chemical potential μ for $\lambda=0.5$ and several values of the SO interaction E_0 . The temperature is $T=0.02\omega_0$ and the energy cutoff is $E_c=100\omega_0$. In the inset n_e is plotted for $\lambda=0$ and for zero temperature.

$$\rho_0(E) = \sum_s \frac{N_s(E)}{2N_0} = \begin{cases} 1 & \text{for } E \geq E_0, \\ \sqrt{\frac{E_0}{E}} & \text{for } E < E_0 \end{cases} \quad (20)$$

is the reduced noninteracting DOS obtained from Eqs. (6) and (7). From the above expressions, it is therefore straightforward to realize the importance on the el-ph properties of the square root singularity of the DOS at low energies. As we shall see in the following, the effective electron mass and the electron spectral properties in the presence of SO interaction will differ qualitatively from the corresponding results for $E_0=0$.

III. EFFECTIVE MASS

The integration over the momenta appearing in Eq. (16) or, equivalently, the integration over the energy in Eq. (19), can be carried out analytically, leaving only the summation over the Matsubara frequency to be performed numerically. Hence, for fixed values of λ , ω_0 and E_0 , the electron self-energy $\Sigma(i\omega_n)$ is obtained by iteration of Eqs. (14)–(16), while Eq. (17) is used to extract the corresponding electron density for a given value of μ . For all cases we have set $E_c=100\omega_0$ and $T=0.02\omega_0$, which is low enough to be representative of the zero temperature case. In Fig. 2 we report the calculated values of n_e , Eq. (18), for $\lambda=0.5$ and for different values of the SO energy E_0 . For comparison, we report in the inset of Fig. 2 the corresponding density values for $\lambda=0$ and at zero temperature. For $E_0=0$, n_e decreases almost linearly as μ is reduced, as expected for a constant DOS in 2D (see inset), but the zero density limit $n_e=0$ (extracted in the $T \rightarrow 0$ limit) is reached only for $\mu=\mu_0 \approx -1.023\omega_0$, which is lower than the noninteracting zero-density value $\mu=0$. This energy decrease represents the ground-state energy of a single electron in interaction with phonons and provides a

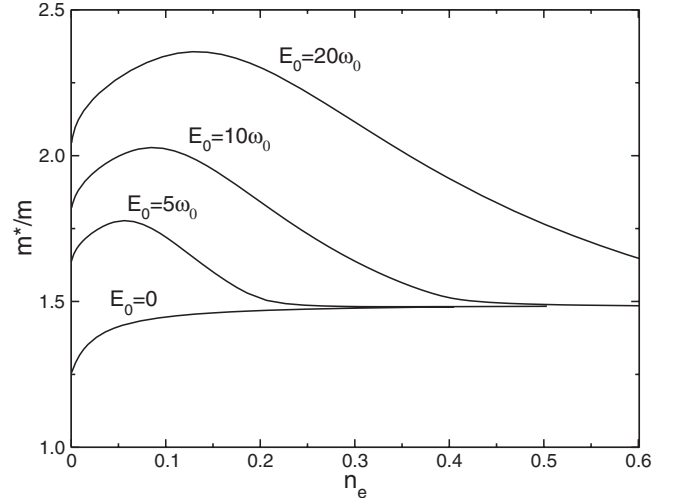


FIG. 3. Electron effective mass m^* as a function of the electron density number n_e for $\lambda=0.5$ and for several values of the SO interaction E_0 .

measure of the strength of the el-ph interaction. For nonzero SO coupling, $E_0 > 0$, two features are apparent in Fig. 2. First, in the low density limit, n_e is no longer a linear function of μ and, second, the ground state energy μ_0 is even more lowered with respect to the $E_0=0$ case. This latter feature indicates that, for fixed λ , a single electron is more strongly coupled to phonons as E_0 increases.

A more quantitative estimation of the role of SO coupling on the el-ph properties is given by the electron effective mass enhancement m^*/m . This quantity can be evaluated from

$$\frac{m^*}{m} = 1 - \left. \frac{\text{Im} \Sigma(i\omega_n)}{\omega_n} \right|_{n=0} \quad (21)$$

provided sufficiently low temperatures are considered. We have checked that for $T=0.02\omega_0$ the effective mass ratio extracted from Eq. (21) is in very good accord with the mass enhancement obtained from the real frequency self-energy (see next section). In Fig. 3 we report our results for m^*/m as a function of the electron number density n_e for the same parameter values of Fig. 2. For $E_0=0$ we obtain the typical trend for a 2D electron gas in the noncrossing approximation: m^*/m is almost a constant and approximately equal to the Migdal-Eliashberg result $1+\lambda$ for relatively large densities while, for $n_e \rightarrow 0$, m^*/m decreases towards the one electron result.²⁹ For $E_0=5\omega_0$, the mass enhancement follows the $E_0=0$ case for densities larger than $n_e \approx 0.2$, corresponding to the range of densities for which n_e is proportional to μ (see Fig. 2). Instead, for lower values of n_e , m^*/m increases up to a maximum and eventually decreases again as $n_e \rightarrow 0$. Higher values of E_0 emphasize the same trend, with higher and broader maxima of m^*/m as E_0 increases.

The results plotted in Fig. 3 clearly show how the underlying diverging DOS, Eq. (20), for $E_0 \neq 0$ is responsible for the enhancement of the effective mass. By reading off from Fig. 2 the values of μ corresponding to the density values for which m^*/m deviates from $1+\lambda$, it is easy to realize that the enhancement of m^*/m starts when μ becomes lower than

$\sim E_0$, that is when the (bare) DOS diverges as $\sqrt{E_0/E}$. In this situation, the coupling to the phonons is no longer parametrized by λ alone, but rather by an effective coupling which takes into account the strongly varying DOS at low energies.³⁰ As a matter of fact, for small λ , by enhancing E_0 the system crosses over from a weak to a strong coupling regime, where the mass enhancement can be considerably larger than unity. It becomes therefore natural to consider signatures of such SO induced strong el-ph coupling regime also in the spectral properties of the electrons, which can provide valuable information testable by tunneling and/or photoemission experiments.^{23,24,26}

IV. SPECTRAL PROPERTIES

The self-energy for real frequencies could be obtained directly from analytical continuation on the real axis of Eqs. (14)–(16). However, since convergence is faster on the imaginary axis, in this paper we opt for the more efficient method of analytical continuation formulated in Ref. 31. Hence, once $\Sigma(i\omega_n)$ has been determined from the imaginary axis equations (14)–(16), the retarded self-energy $\Sigma_R(\omega) = \Sigma(\omega + i\delta)$ follows from

$$\begin{aligned} \Sigma_R(\omega) = & -T\lambda \sum_m D(\omega - i\omega_m)g(i\omega_m) \\ & + \lambda \frac{\omega_0}{2} [n(\omega_0) + f(\omega_0 - \omega)]g_R(\omega - \omega_0) \\ & + \lambda \frac{\omega_0}{2} [n(\omega_0) + f(\omega_0 + \omega)]g_R(\omega + \omega_0), \quad (22) \end{aligned}$$

where $g_R(\omega \pm \omega_0) = g(\omega \pm \omega_0 + i\delta)$ and $n(x)$ and $f(x)$ are the distribution functions for bosons and fermions, respectively. The real and imaginary parts of $\Sigma_R(\omega)$ are plotted in Fig. 4 for $\lambda=0.5$, $n_e=0.1$, $E_0=0$ [Fig. 4(a)], and $E_0=5\omega_0$ [Fig. 4(b)]. The mass enhancement extracted from $m^*/m = \lim_{\omega \rightarrow 0} [1 - d\text{Re} \Sigma_R(\omega)/d\omega]$ is 1.45 for $E_0=0$ and 1.72 for $E_0=5\omega_0$, which agree with the m^*/m values plotted in Fig. 3. For $E_0=0$, the self-energy displays features typical of the Holstein model for a 2D system in the noncrossing approximation. Namely, $\text{Im} \Sigma_R(\omega) = 0$ for $|\omega| < \omega_0$, while at larger frequencies $\text{Im} \Sigma_R(\omega) \simeq -\pi\lambda\omega_0/2$. The rapid decrease of $|\text{Im} \Sigma_R(\omega)|$ at negative frequencies stems from the bottom band edge. For $E_0=5\omega_0$ [Fig. 4(b)] the structure of $\Sigma_R(\omega)$ is more intricate due to the strong energy dependence of the underlying bare DOS. In fact, for $n_e=0.1$, the value of the (bare) chemical potential μ is well below $E_0=5\omega_0$ (see Fig. 2), and the ω dependence of $\Sigma_R(\omega)$ becomes strongly influenced by the square-root divergence of the DOS. This is particularly clear in Fig. 4(b), where $\text{Im} \Sigma(\omega)$ reproduces for $\omega < 0$ the low-energy profile of the DOS shifted by multiples of ω_0 . This feature is characteristic of a strongly-coupled el-ph system and is fully consistent with the high value of the mass enhancement ($m^*/m \simeq 1.72$) for this particular case.

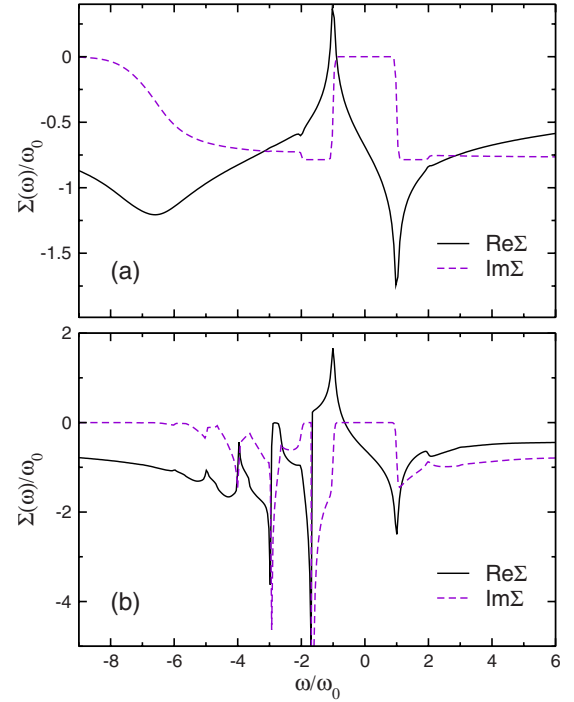


FIG. 4. (Color online) Real and imaginary parts of the electron self-energy for $\lambda=0.5$ and electron density $n_e=0.1$. The SO energy is $E_0=0$ in (a) and $E_0=5\omega_0$ in (b).

A global view of the behavior for several values of the electron number density and of the SO energy is given in Fig. 5 where the reduced DOS for the interacting system

$$\rho(\omega) = -\frac{1}{\pi} \text{Im} g_R(\omega) \quad (23)$$

is plotted for fixed $\lambda=0.5$. For comparison, we also report the bare DOS $\rho_0(\omega)$, Eq. (20), for the corresponding values of n_e and E_0 . For $E_0=0$, Fig. 5(a), reducing the electron density merely shifts the Fermi level for the interacting electron (vertical dotted line) towards the bottom of the band. For $|\omega| < \omega_0\rho(\omega)$ coincides with the bare reduced DOS $\rho_0(\omega)=1$ because, as also shown in Fig. 4, the imaginary part of the self-energy is zero in that frequency range. Compared to the $\lambda=0$ case, whose DOS has a finite step at the bottom of the band, the profile of $\rho(\omega)$ is smeared by the el-ph interaction. A similar feature is obtained also for $E_0=5\omega_0$ [Fig. 5(b)] and $n_e=0.3$ where, now, the square-root divergence of $\rho_0(\omega)$ is rounded-off in $\rho(\omega)$ due to the finite lifetime for $\lambda=0.5$. However, contrary to the $E_0=0$ case, reducing n_e does not translate to a (more or less) rigid shift of the Fermi level but, rather, creates new structures whose intensity increases as the Fermi level moves deeper into the square-root singularity of $\rho_0(\omega)$. This is even more pronounced for $E_0=10\omega_0$ and $E_0=20\omega_0$ plotted, respectively, in Figs. 5(c) and 5(d). For the latter cases, the profile of $\rho(\omega)$ for $n_e=0.1$ is characterized by well defined peaks separated by multiples of ω_0 , and whose widths decrease as E_0/ω_0 is enhanced.

Such strong-coupling features are, in principle, directly observable by means of low-temperature tunneling or photo-

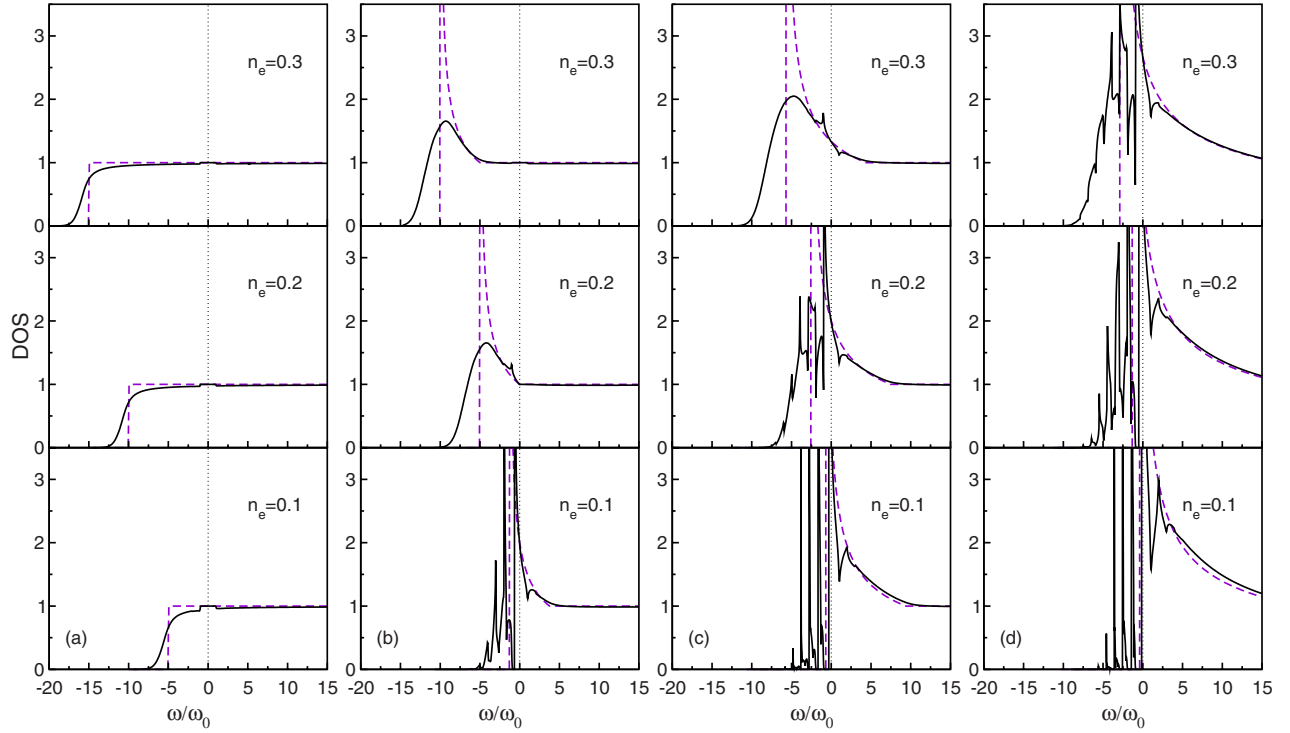


FIG. 5. (Color online) Reduced DOS for $\lambda=0.5$ (solid lines) and $\lambda=0$ (dashed lines). The vertical dotted line at $\omega=0$ indicates the Fermi level. The cutoff energy is $E_c=100\omega_0$ and the temperature is $T=0.02\omega_0$ for the interacting cases ($T=0$ for $\lambda=0$). (a) $E_0=0$, (b) $E_0=5\omega_0$, (c) $E_0=10\omega_0$, (d) $E_0=20\omega_0$.

emission measurements provided, however, that other interactions do not alter significantly the profile of $\rho(\omega)$. This could be not the case, for example, when disorder effects are taken into account, since these tend to smear all sharp features of the DOS even at zero temperature. To investigate this point, we have considered a coupling to a short-range impurity potential of the form $V(\mathbf{r})=V_{\text{imp}}\sum_i\delta(\mathbf{r}-\mathbf{R}_i)$, where \mathbf{R}_i are the random positions of impurity scatterers. Within the self-consistent Born approximation, the resulting self-energy is hence given by Eq. (15) with the impurity term $\Gamma_{\text{imp}}g(i\omega_n)/\pi$ added in the right-hand side, and Eq. (22) modified accordingly. The parameter $\Gamma_{\text{imp}}=1/2\tau_{\text{imp}}=\pi n_i V_{\text{imp}}^2 N_0$ is the usual scattering rate for zero SO coupling and for density n_i of impurities. In Fig. 6 we report the calculated reduced DOS $\rho(\omega)$ for $\lambda=0.5$, $E_0=10\omega_0$, $n_e=0.1$, and for several values of Γ_{imp} . Also plotted by dashed lines for $\Gamma_{\text{imp}}\neq 0$ are the corresponding DOS curves in the absence of el-ph interaction ($\lambda=0$). Compared to the clean limit $\Gamma_{\text{imp}}=0$ (top panel), for rather weak disorder ($\Gamma_{\text{imp}}=0.02E_0$) the phonon peaks at $\omega<0$ are considerably less sharp and slightly shifted at more negative frequencies, but nevertheless still clearly discernible. Larger values of Γ_{imp} increasingly smear the phonon structures, and gradually the peaks disappear. For $\Gamma_{\text{imp}}=0.2E_0$ (which corresponds to $\Gamma_{\text{imp}}=2\omega_0$) the resulting DOS is basically dominated by the impurity interaction, and does not deviate much from the $\lambda=0$ case.

V. DISCUSSION

In this section we review the meaning of the approximations used in the present work and discuss alternative models

for the study of the el-ph interaction in strong Rashba SO systems. Let us start by considering the limitations of the noncrossing approximation for the electron self-energy. For zero SO interaction, or for Fermi energies sufficiently larger than E_0 , this is a rather good description of the el-ph problem provided λ is sufficiently small. However, as we have seen, for nonzero SO interaction the electrons behave as effectively strongly coupled to the phonons when the Fermi level is below E_0 . This is because of the square-root singularity in the DOS when $E_0\neq 0$. In the $E_F<E_0$ regime, therefore, the noncrossing approximation, although making evident the trend towards strong coupling, may not be adequate for a more trustworthy description of the system. It is instructive at this point to consider the limiting situation where only one electron is present. By using second-order perturbation theory (that is simply the noncrossing approximation with the bare electron Green's function) it is easy to evaluate the mass enhancement factor. At zero temperature, and setting for simplicity $E_c/E_0=\infty$, this is given by

$$\frac{m^*}{m} = 1 + \frac{\lambda}{2} + \frac{\lambda}{2} \sqrt{\frac{E_0}{\omega_0}} \arctan\left(\sqrt{\frac{E_0}{\omega_0}}\right). \quad (24)$$

It is clear from the above expression that for $E_0\gg\omega_0$ the mass enhancement factor is governed by an effective coupling, say $\tilde{\lambda}$, proportional to $\lambda\sqrt{E_0/\omega_0}$, amplified with respect to λ by the square-root divergent DOS. Equation (24) clarifies also that the relevant adiabatic parameter for $E_F\ll E_0$ is ω_0/E_0 , rather than ω_0/E_c (where E_c plays the role of the bandwidth), and that the effective coupling $\tilde{\lambda}$ increases as

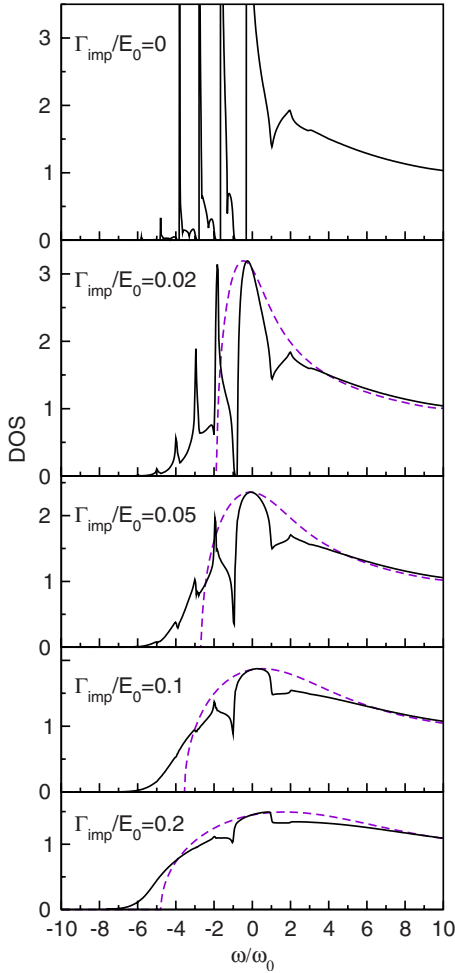


FIG. 6. (Color online) Reduced DOS for $\lambda=0.5$ (solid lines) and $\lambda=0$ (dashed lines) for several values of the impurity scattering rate Γ_{imp} . The temperature is $T=0.02\omega_0$ and $E_0=10\omega_0$, $n_e=0.1$ for all cases.

$\omega_0/E_0 \rightarrow 0$. Consequently, in the adiabatic limit $\omega_0/E_0=0$ perturbation theory breaks down for any finite λ because $\tilde{\lambda} = \infty$. This leads us to suspect that, in analogy with the adiabatic limit of the one-dimensional lattice Holstein model,³² the ground state of a single electron for $\omega_0/E_0=0$ is always a bound polaron. However, for $\omega_0/E_0 \neq 0$, the effective coupling $\tilde{\lambda} \approx \lambda\sqrt{E_0/\omega_0}$ is finite, which permits us to estimate a rough range of validity of Eq. (24). Indeed, contributions of higher orders of perturbation theory become negligible as long as $\tilde{\lambda} \ll 1$, corresponding to $\lambda \ll \sqrt{\omega_0/E_0}$, consistent with the results on the one-dimensional Holstein model of Refs. 33 and 34, which show better agreement between perturbation theory and exact diagonalization results as ω_0 increases.

Also for low but finite electron densities it is possible to interpret the coupling to the phonons in terms of an effective el-ph coupling $\tilde{\lambda}$ which grows as E_0 increases. For example, in the range of electron densities $n_e=0.1-0.2$, the mass enhancement factor plotted in Fig. 3 for $\lambda=0.5$ may be interpreted by an effective Migdal-Eliashberg formula $m^*/m=1+\tilde{\lambda}$, where $\tilde{\lambda} \approx 1$ for $E_0=10\omega_0$ and $\tilde{\lambda} \approx 1.3$ for $E_0=20\omega_0$.

However, contrary to the one-electron case discussed above, now $\tilde{\lambda}$ depends on the Fermi energy E_F . Indeed, provided that $\omega_0 < E_F < E_0$, the effective coupling turns out to be of order $\tilde{\lambda} \approx \lambda\sqrt{E_0/E_F}$, where the square-root term stems from the singularity of the DOS, Eq. (20), in analogy with the general definition of the effective el-ph interaction in the presence of a van Hove singularity.³⁵ At this point it is possible to estimate the validity of the self-consistent noncrossing approximation for the self-energy considered in the previous sections. In fact, according to Migdal's theorem generalized to systems with diverging DOS,³⁵ the el-ph vertex correction factors beyond the noncrossing approximation are at least of order $P=\tilde{\lambda}\omega_0/E_F$, so that neglecting them would introduce an error of order P . Estimates of P for the different cases discussed in this paper can be obtained by evaluating $\tilde{\lambda} \approx 1-m^*/m$ from Fig. 3. In this way the Fermi energy is roughly given by $E_F \approx (\lambda/\tilde{\lambda})^2 E_0$, which then can be inserted in the definition of P . For the low density value $n_e=0.1$ we find $P \geq 1$ for $E_0=20\omega_0$ and $P \approx 0.5$ for $E_0=10\omega_0$, showing that the noncrossing approximation is quantitatively inaccurate in this case. However, already for $n_e=0.2$, for which effectively strong-coupling features are apparent from Figs. 3 and 4, the contributions of the vertex corrections drop to $P \approx 0.4$ and $P \approx 0.2$ for $E_0=20\omega_0$ and $E_0=10\omega_0$, respectively. In this situation, the noncrossing approximation is fairly reliable and its accuracy improves as n_e is further enhanced and/or E_0/ω_0 is reduced.

Let us turn now to discuss the general form of the self-energy for the case in which the el-ph matrix element is momentum dependent. Here we consider the situation in which the momentum dependence is only through the modulus q of the momentum transfer \mathbf{q} , as is the case, for example, with the 2D Fröhlich model, for which the coupling goes as $1/\sqrt{q}$. As shown in the Appendix, a fully general expression of the self-energy valid also beyond the noncrossing approximation is

$$\Sigma(\mathbf{k}, i\omega_n) = \Sigma_1(k, i\omega_n)\mathbf{1} + \Sigma_2(k, i\omega_n)\hat{\Omega}_{\mathbf{k}} \cdot \boldsymbol{\sigma}, \quad (25)$$

where Σ_1 and Σ_2 are scalars. Compared to Eq. (15), the above expression has an additional term which is off-diagonal in the spin subspace, renormalizing therefore the SO coupling. This term disappears ($\Sigma_2=0$) only when the el-ph matrix element is momentum independent, as in the Holstein model, and at the same time the self-energy is evaluated in the noncrossing approximation. In all other cases, such as, e.g., the Fröhlich model in the noncrossing approximation, Σ_2 is nonzero. For sufficiently large values of E_F , such that the weak SO limit $E_0/E_F \ll 1$ holds true so that the Fermi level lies far above the 1D singularity of the DOS, Σ_2 turns out to be of order $\lambda\omega\Delta_{SO}/E_F \propto \lambda\omega_0\sqrt{E_0/E_F}$, and can be disregarded in comparison with $\Sigma_1 \approx \lambda\omega_0$. On the contrary, when $E_F/E_0 \leq 1$, Σ_1 and Σ_2 have comparable magnitude, and the full momentum and frequency dependent of both terms must be considered for a consistent evaluation of the el-ph effects.

VI. CONCLUSIONS

In this paper we have addressed the role of the Rashba SO interaction in the properties of a coupled el-ph gas in two dimensions. By using a self-consistent noncrossing approximation for the electron self-energy, we have studied the mass enhancement factor and the spectral properties. We have shown that, for sufficiently strong SO interaction, the electron becomes strongly coupled to the phonons even if el-ph coupling λ can be classified as weak. We identify this behavior as being due to a topological change of the Fermi surface for strong SO interaction, which gives rise to a square-root singularity in the DOS at low energies. Signatures of such effectively strong el-ph coupling are found in the mass enhancement factor, which becomes as large as $m^*/m \approx 2$ for el-ph coupling of only $\lambda=0.5$, and in the energy dependence of the interacting DOS, displaying low energy peaks separated by multiples of the phonon energy ω_0 . This latter feature could be tested experimentally by tunneling or photoemission experiments in systems where the Fermi level can be tuned to approach the square-root singularity of the DOS. We have then discussed limitations of the noncrossing approximation approach and possible generalizations of the theory for momentum-dependent el-ph matrix elements. Since the problem of el-ph coupling in the presence of SO interaction is relevant for several systems such as metal and semimetal surface states, surface superconductors, or low-dimensional heterostructures, and given the current interest in spintronic physics, we hope that our work will stimulate further investigations.

APPENDIX

In this appendix we evaluate the form of the electron self-energy when the el-ph interaction is momentum dependent. In particular, we consider the Hamiltonian $H=H_0+H_{\text{ph}}$, where H_0 is the Rashba spin-orbit Hamiltonian of Eq. (1) and

$$H_{\text{ph}} = \sum_{\mathbf{q}} \omega_0 a_{\mathbf{q}}^\dagger a_{\mathbf{q}} + \sum_{\mathbf{k}\mathbf{k}'\alpha} g_{\mathbf{k}-\mathbf{k}'} c_{\mathbf{k}\alpha}^\dagger c_{\mathbf{k}'\alpha} (a_{\mathbf{k}-\mathbf{k}'}^\dagger + a_{\mathbf{k}'-\mathbf{k}}), \quad (\text{A1})$$

where $g_{\mathbf{q}}$ is the el-ph matrix element which we assume depends only on the modulus of momentum transfer \mathbf{q} . It is convenient to rewrite H in terms of the eigenvectors of H_0 , whose annihilation operators $d_{\mathbf{k}s}$ ($s=\pm$) are related to $c_{\mathbf{k}\alpha}$ through

$$\begin{pmatrix} d_{\mathbf{k}+} \\ d_{\mathbf{k}-} \end{pmatrix} = \mathbf{T}_{\mathbf{k}} \begin{pmatrix} c_{\mathbf{k}\uparrow} \\ c_{\mathbf{k}\downarrow} \end{pmatrix} = \frac{1}{\sqrt{2}} \begin{pmatrix} 1 & -ie^{-i\varphi} \\ 1 & ie^{-i\varphi} \end{pmatrix} \begin{pmatrix} c_{\mathbf{k}\uparrow} \\ c_{\mathbf{k}\downarrow} \end{pmatrix}, \quad (\text{A2})$$

where φ is the azimuthal angle of \mathbf{k} . In this basis, H_0 is diagonal with dispersion relation given by Eq. (3) while H_{ph} becomes

$$H_{\text{ph}} = \sum_{\mathbf{q}} \omega_0 a_{\mathbf{q}}^\dagger a_{\mathbf{q}} + \sum_{\mathbf{k}\mathbf{k}'s's'} M_{\mathbf{k}-\mathbf{k}'}^{s,s'} d_{\mathbf{k}s}^\dagger d_{\mathbf{k}'s'} (a_{\mathbf{k}-\mathbf{k}'}^\dagger + a_{\mathbf{k}'-\mathbf{k}}), \quad (\text{A3})$$

with

$$M_{\mathbf{k}-\mathbf{k}'}^{s,s'} = g_{\mathbf{k}-\mathbf{k}'} \frac{1 + ss' e^{i(\varphi-\varphi')}}{2}. \quad (\text{A4})$$

By applying Wick's theorem, it turns out that, to all orders of the el-ph interaction, the Green's function in the chiral basis has zero off-diagonal components so that, if $G_{\pm}(\mathbf{k}, \tau) = -\langle T_{\tau} d_{\mathbf{k}\pm}(\tau) d_{\mathbf{k}\pm}^\dagger(0) \rangle$, the matrix Green's function in the original spin subspace becomes

$$\begin{aligned} \mathbf{G}(\mathbf{k}, i\omega_n) &= \mathbf{T}_{\mathbf{k}}^\dagger \begin{pmatrix} G_+(\mathbf{k}, i\omega_n) & 0 \\ 0 & G_-(\mathbf{k}, i\omega_n) \end{pmatrix} \mathbf{T}_{\mathbf{k}} \\ &= \frac{1}{2} \sum_{s=\pm} (1 + s \hat{\Omega}_{\mathbf{k}} \cdot \sigma) G_s(\mathbf{k}, i\omega_n). \end{aligned} \quad (\text{A5})$$

Consequently, by using Dyson's equation (9), the matrix self-energy in the spin subspace is

$$\Sigma(\mathbf{k}, i\omega_n) = \Sigma_1(\mathbf{k}, i\omega_n) 1 + \Sigma_2(\mathbf{k}, i\omega_n) \hat{\Omega}_{\mathbf{k}} \cdot \sigma, \quad (\text{A6})$$

where

$$\Sigma_{1(2)}(\mathbf{k}, i\omega_n) = \frac{\Sigma_+(\mathbf{k}, i\omega_n) + (-)\Sigma_-(\mathbf{k}, i\omega_n)}{2}. \quad (\text{A7})$$

In order to obtain Eq. (25), it suffices to demonstrate that the momentum dependence of self-energy in the chiral basis $\Sigma_{\pm}(\mathbf{k}, i\omega_n)$ is only via $k=|\mathbf{k}|$. This is accomplished by noticing that the el-ph matrix element in the chiral basis (A4), depends on the direction of the momentum transfer $\mathbf{k}-\mathbf{k}'$ solely through $\varphi-\varphi'$. Hence, if the electronic dispersion depends only on the modulus of the momentum, as is the case with Eq. (3), a general self-energy diagram in the chiral basis will be independent of the direction of \mathbf{k} which, by using Eq. (A7), is consistent with Eq. (25).

¹G. Prinz, Phys. Today **48**, 58 (1995).

²I. Žutić, J. Fabian, and S. Das Sarma, Rev. Mod. Phys. **76**, 323 (2004).

³E. I. Rashba, Sov. Phys. Solid State **2**, 1224 (1960).

⁴G. Dresselhaus, Phys. Rev. **100**, 580 (1955).

⁵X. C. Zhang, A. Pfeuffer-Jeschke, K. Ortner, V. Hock, H. Buhmann, C. R. Becker, and G. Landwehr, Phys. Rev. B **63**, 245305 (2001).

⁶Y. S. Gui, C. R. Becker, N. Dai, J. Liu, Z. J. Qiu, E. G. Novik, M. Schafer, X. Z. Shu, J. H. Chu, H. Buhmann, and L. W. Molenkamp, Phys. Rev. B **70**, 115328 (2004).

⁷S. LaShell, B. A. McDougall, and E. Jensen, Phys. Rev. Lett. **77**, 3419 (1996).

⁸Yu. M. Koroteev, G. Bihlmayer, J. E. Gayone, E. V. Chulkov, S. Blugel, P. M. Echenique, and P. Hofmann, Phys. Rev. Lett. **93**, 046403 (2004).

- ⁹K. Sugawara, T. Sato, S. Souma, T. Takahashi, M. Arai, and T. Sasaki, *Phys. Rev. Lett.* **96**, 046411 (2006).
- ¹⁰J. R. McLaughlan, E. M. Llewellyn-Samuel, and S. Crampin, *J. Phys.: Condens. Matter* **16**, 6841 (2004).
- ¹¹E. Rotenberg, J. W. Chung, and S. D. Kevan, *Phys. Rev. Lett.* **82**, 4066 (1999).
- ¹²D. Pacilé, C. R. Ast, M. Papagno, C. Da Silva, L. Moreschini, M. Falub, A. P. Seitsonen, and M. Grioni, *Phys. Rev. B* **73**, 245429 (2006).
- ¹³C. R. Ast, G. Wittich, P. Wahl, R. Vogelgesang, D. Pacilé, M. C. Falub, L. Moreschini, M. Papagno, M. Grioni, and K. Kern, *Phys. Rev. B* **75**, 201401(R) (2007).
- ¹⁴C. R. Ast, J. Henk, A. Ernst, L. Moreschini, M. C. Falub, D. Pacilé, P. Bruno, K. Kern, and M. Grioni, *Phys. Rev. Lett.* **98**, 186807 (2007).
- ¹⁵I. Barke, F. Zheng, T. K. Rügheimer, and F. J. Himpsel, *Phys. Rev. Lett.* **97**, 226405 (2006).
- ¹⁶E. Bauer, G. Hilscher, H. Michor, C. Paul, E. W. Scheidt, A. Griбанov, Y. Seropegin, H. Noel, M. Sgrist, and P. Rogl, *Phys. Rev. Lett.* **92**, 027003 (2004).
- ¹⁷K. V. Samokhin, E. S. Zijlstra, and S. K. Bose, *Phys. Rev. B* **69**, 094514 (2004).
- ¹⁸K. Togano, P. Badica, Y. Nakamori, S. Orimo, H. Takeya, and K. Hirata, *Phys. Rev. Lett.* **93**, 247004 (2004).
- ¹⁹H. Q. Yuan, D. F. Agterberg, N. Hayashi, P. Badica, D. Vandervelde, K. Togano, M. Sgrist, and M. B. Salamon, *Phys. Rev. Lett.* **97**, 017006 (2006).
- ²⁰C. R. Ast, D. Pacilé, M. Falub, L. Moreschini, M. Papagno, G. Wittich, P. Wahl, R. Vogelgesang, M. Grioni, and K. Kern, arXiv:cond-mat/0509509 (unpublished).
- ²¹A. V. Chaplik and L. I. Magarill, *Phys. Rev. Lett.* **96**, 126402 (2006).
- ²²E. Cappelluti, C. Grimaldi, and F. Marsiglio, *Phys. Rev. Lett.* **98**, 167002 (2007).
- ²³J. E. Gayone, S. V. Hoffmann, Z. Li, and Ph. Hofmann, *Phys. Rev. Lett.* **91**, 127601 (2003).
- ²⁴Ph. Hofmann, *Prog. Surf. Sci.* **81**, 191 (2006).
- ²⁵S. LaShell, B. A. McDougall, and E. Jensen, *Phys. Rev. B* **74**, 033410 (2006).
- ²⁶J. Kröger, *Rep. Prog. Phys.* **69**, 899 (2006).
- ²⁷L. P. Gor'kov, *Int. J. Mod. Phys. B* **20**, 2569 (2006).
- ²⁸A. A. Abrikosov, L. P. Gorkov, and I. E. Dzyaloshinsky, *Methods of Quantum Field Theory in Statistical Physics* (Dover, New York, 1975).
- ²⁹E. Cappelluti, S. Ciuchi, C. Grimaldi, and L. Pietronero, *Phys. Rev. B* **68**, 174509 (2003).
- ³⁰S. Ciuchi, F. de Pasquale, S. Fratini, and D. Feinberg, *Phys. Rev. B* **56**, 4494 (1997).
- ³¹F. Marsiglio, M. Schossmann, and J. P. Carbotte, *Phys. Rev. B* **37**, 4965 (1988).
- ³²V. V. Kabanov and O. Yu. Mashtakov, *Phys. Rev. B* **47**, 6060 (1993). See also discussion in Ref. 30.
- ³³F. Marsiglio, *Phys. Lett. A* **180**, 280 (1993).
- ³⁴M. Capone, S. Ciuchi, and C. Grimaldi, *Europhys. Lett.* **42**, 523 (1998).
- ³⁵E. Cappelluti and L. Pietronero, *Phys. Rev. B* **53**, 932 (1996).